

# Heavy Higgs Boson Production at Colliders in the Singlet-Triplet Scotogenic Dark Matter Model

---

Marco Aurelio Díaz<sup>a</sup> Nicolás Rojas<sup>b</sup> Sebastián Urrutia-Quiroga<sup>a</sup> José W. F. Valle<sup>b</sup>

<sup>a</sup>*Instituto de Física, Pontificia Universidad Católica de Chile,  
Avenida Vicuña Mackenna 4860, Santiago, Chile.*

<sup>b</sup>*Instituto de Física Corpuscular CSIC/Universitat de Valencia,  
Parc Científic, calle Catedrático José Beltrán, 2, E-46980 Paterna, Spain.*

## ABSTRACT:

We consider the possibility that the dark matter particle is a scalar WIMP messenger associated to neutrino mass generation, made stable by the same symmetry responsible for the radiative origin of neutrino mass. We focus on some of the implications of this proposal as realized within the singlet-triplet scotogenic dark matter model. We identify parameter sets consistent both with neutrino mass and the observed dark matter abundance. Finally we characterize the expected phenomenological profile of heavy Higgs boson physics at the LHC as well as at future linear Colliders.

**KEYWORDS:** Heavy Higgs Production, Collider Production, Dark Matter, Scotogenic Mechanism.

ARXIV EPRINT: [1612.06569](https://arxiv.org/abs/1612.06569)

---

## Contents

<b>1</b>	<b>Introduction</b>	<b>1</b>
<b>2</b>	<b>Generalities About Singlet Triplet Scotogenic Model</b>	<b>3</b>
2.1	The Model and the New Fermions	3
2.2	Radiative Neutrino Masses	4
<b>3</b>	<b>The Scalar Sector of the Model</b>	<b>5</b>
3.1	The Scalar Potential	5
3.2	The Scalar Mass Spectrum	7
<b>4</b>	<b>Numerical Analysis</b>	<b>9</b>
4.1	Parameter Space	9
4.1.1	Neutrino mass	9
4.1.2	Relic density	10
4.2	Production of heavy Higgs boson	13
4.2.1	Two benchmark points	13
4.2.2	Decay Rates for the Charged and Heavy CP-Even Higgs	17
<b>5</b>	<b>Conclusions</b>	<b>18</b>
<b>A</b>	<b>Appendix : Feynman Rules for Decay Channels</b>	<b>19</b>
A.1	Diagrams Involving Neutral Higgses	19
A.2	Diagrams Involving Charged Higgses	22

---

## 1 Introduction

Particle physics has celebrated two well-deserved Nobel prizes in this decade. These were associated to the historic discoveries of the Higgs boson [1] at the Large Hadron Collider (LHC) and of neutrino oscillations using solar and atmospheric neutrinos [2, 3] beautifully confirmed by laboratory experiments based at reactors and accelerators [4]. Though these discoveries culminate decades of thriving searches, by no means they close our efforts to understand what lies behind these phenomena [5]. There are, in addition, robust hints from cosmology as to the incompleteness of the Standard Model. For example, there is a growing

evidence in favor of the existence of non-baryonic dark matter [6], which also indicates the need for new physics. Underpinning the elusive nature of dark matter constitutes a most important challenge in astroparticle physics and modern cosmology. A popular dark matter candidate is a weakly interacting massive particle (WIMP), such as the lightest supersymmetric particle, typically a neutralino, present in supersymmetric models with R parity conservation. WIMPs can naturally account for the required relic density thermally and be detectable by nuclear recoil through weak strength interactions.

Irrespective of the existence of supersymmetry in nature, the problem of neutrino mass and the explanation of dark matter may have a common origin, so that the dark matter candidate can be closely associated with the mechanism of neutrino mass generation. For example dark matter stability may be a remnant of the same symmetry which accounts for the observed pattern of neutrino oscillations [7, 8, 9]. In this case, the symmetry stabilizing the lightest particle charged under it, gives rise to a WIMP Dark Matter candidate. Another possibility, recently proposed in [10], is that the dark matter candidate is a scalar WIMP, and its stability emerges from a symmetry enforcing the Dirac nature of neutrinos. In another broad class of models the dark matter candidate appears as a pseudo-Goldstone boson associated to neutrino mass generation, an old idea [11] which, in its original realization, leads to warm decaying dark matter. In this case dark matter may be detected through subtle effects in the cosmic microwave background [12] as well as indirectly through X-ray and gamma-ray line searches in the sky [13, 14].

In this paper we focus on the case of Scotogenic Models, a beautiful idea proposed by Ernest Ma [15] and generalized in Ref. [16]. The dark matter can be either scalar or fermionic and can be interpreted as the radiative messenger neutrino mass generation. This postulates that the same symmetry which is responsible for the radiative nature of neutrino masses also stabilizes dark matter which emerges as the WIMP messenger of neutrino mass generation. Here we focus on the possibility of scalar scotogenic DM since the fermionic case has been considered in [16]. In Sec. 2 we describe the main aspects of the model such as the Yukawa sector and the symmetry responsible for radiative neutrino masses. In Sec. 3 we describe the scalar sector in detail, including the identification of the relevant parameter space consistent, e.g. with neutrino mass and an adequate dark matter relic density. The resulting scalar mass spectrum, including the dark matter sector is derived. The results of our numerical study of Higgs boson production cross section at the LHC as well as at the proposed CLIC and ILC options are given in Sec. 4. Moreover we give the predicted charged as well as heavy CP-even Higgs boson decay rates. Finally, we conclude in Sec. 5, and in the appendix we collect the Feynman rules for the various decays heavy scalars present in the model.

## 2 Generalities About Singlet Triplet Scotogenic Model

### 2.1 The Model and the New Fermions

The model we will work was proposed at [16]. Its particle content, with the respective quantum numbers, is given at the table 1. As in other Scotogenic Models, the  $\mathbb{Z}_2$  symmetry plays the role of a stabilizing symmetry for the dark matter candidate and for ensuring radiative generation of neutrino masses. The most general  $SU(3)_c \times SU(2)_L \times U(1)_Y$ , Lorentz and

	Standard Model			new fermions		new scalars	
	$L$	$e$	$\phi$	$\Sigma$	$N$	$\eta$	$\Omega$
$SU(2)_L$	2	1	2	3	1	2	3
$U(1)_Y$	-1/2	-1	1/2	0	0	1/2	0
$\mathbb{Z}_2$	+	+	+	-	-	-	+
$L$	1	1	0	0	0	-1	0

**Table 1.** Fields of the STSM and their quantum numbers.

$\mathbb{Z}_2$  invariant Yukawa Lagrangian is given by

$$-\mathcal{L}_Y = Y_e^{\alpha\beta} \overline{L}_\alpha \phi e_\beta + Y_N^\alpha \overline{L}_\alpha i\sigma_2 \eta^* N + Y_\Sigma^\alpha \overline{L}_\alpha C \Sigma^\dagger i\sigma_2 \eta^* + Y_\Omega \text{Tr}(\overline{\Sigma} \Omega) N + h.c. \quad (2.1)$$

where the greek indices stand for lepton generations. The symbol  $\sigma_2$  is the second Pauli matrix in order to conjugate the  $SU(2)_L \times U(1)_Y$  charges and  $C$  is the Lorentz charge conjugation matrix. The new Yukawas couplings  $Y_N^\alpha$  and  $Y_\Sigma^\alpha$  parametrize the interactions between new scalars, new fermions and SM leptons. Moreover, they take part in the neutrino mass generation mechanism.

On the other hand, the new fermions  $N$  and  $\Sigma$  have Majorana mass terms, which are given by:

$$-\mathcal{L}_M = \frac{1}{2} M_\Sigma \text{Tr}(\overline{\Sigma}^c \Sigma) + \frac{1}{2} M_N \overline{N}^c N + h.c. \quad (2.2)$$

where the superindex  $c$  stands for the Lorentz charge conjugation in order to get an invariant Lagrangian. Notice that, after electroweak symmetry breaking, the Yukawa coupling  $Y_\Omega$  mixes the neutral component of  $\Sigma$  with  $N$ . Thus the mass sector for the neutral fermions is given by

$$\mathcal{M}_x = \begin{bmatrix} M_\Sigma & Y_\Omega v_\Omega \\ Y_\Omega v_\Omega & M_N \end{bmatrix}. \quad (2.3)$$

Hence one can define the mass eigenstates  $\zeta_{1,2}$  for the pair  $(\Sigma_0, N)$  as

$$\begin{bmatrix} \zeta_1 \\ \zeta_2 \end{bmatrix} = \begin{bmatrix} \cos \theta & \sin \theta \\ -\sin \theta & \cos \theta \end{bmatrix} \begin{bmatrix} \Sigma^0 \\ N \end{bmatrix} = V(\theta) \begin{bmatrix} \Sigma^0 \\ N \end{bmatrix}, \quad (2.4)$$

With this definition at hand, one can write down also the Yukawas for these eigenstates as follows:

$$h = \begin{bmatrix} \frac{Y_\Sigma^1}{\sqrt{2}} & Y_N^1 \\ \frac{Y_\Sigma^2}{\sqrt{2}} & Y_N^2 \\ \frac{Y_\Sigma^3}{\sqrt{2}} & Y_N^3 \end{bmatrix} \cdot V^T(\theta), \quad (2.5)$$

A definition that will prove to be useful for the radiative generation of neutrino masses. Notice that, as shown previously [16], the lightest of these states is a suitable WIMP-like dark matter candidate. Nevertheless, in what follows we will assume a scalar dark matter candidate made up of the lightest real neutral component of the  $\eta$  field (namely  $\eta_R$ ). This has similar features to Higgs portal WIMP dark matter, although this model allows tree level interactions of the field  $\eta$  with the SM through leptons as well, as seen from eq. (2.1). This is a possible way of distinguishing this model from the Inert Higgs Dark Matter (IHDM) scenario in which the *inert* doublet has no Yukawa interaction with either leptons or quarks.

## 2.2 Radiative Neutrino Masses

Here we will briefly introduce the mechanism that gives rise to radiative neutrino mass generation. This depends also on parameters in the scalar potential, something that we will discuss in detail below. As already mentioned, the  $\mathbb{Z}_2$  symmetry is in charge of ensuring the radiative nature of neutrino masses. The mechanism forbids the  $\eta$  field from getting a vacuum expectation value (vev) because the  $\mathbb{Z}_2$  symmetry is exactly conserved, in such a way that the Yukawa terms  $L\eta N$  and  $L\Sigma\eta$  do not produce neutrino mass at tree level. Hence neutrino masses are indeed radiatively induced.

If we include just one of the new fermion fields, either  $\Sigma$  or  $N$ , one of the columns at the Yukawa matrix (2.5) gets removed, so that we will be left with a neutrino mass matrix that has two zero eigenvalues. However, a setup with one  $\Sigma$  and one of  $N$  will lead us to two massive neutrinos and one massless neutrino. This is enough to account for current oscillation data [4]. The contributions for radiative neutrino masses are shown at figure 1.

In the figure, we notice the key role of the quartic coupling  $\lambda''_{\phi\eta}$ , since it is related to the conservation of lepton number. While this number has no unique assignment within the model, regardless of the choice, it is not a conserved quantity in the Lagrangian. The lepton number assignment we will use throughout the paper is shown in the last row at table 1, in which the  $\eta$  field has lepton number  $-1$ . Here, the coupling  $\lambda''_{\phi\eta} (\phi^\dagger\eta)^2$  breaks lepton number explicitly, and induces Majorana neutrino masses through the loop in figure 1<sup>1</sup>. Since lepton

---

<sup>1</sup>An alternative assignment would be when  $\Sigma$  and  $N$  carry lepton number so that the Yukawa interactions at Eq. (2.1) do conserve this number, however, the Majorana masses at Eq. (2.2) do not.

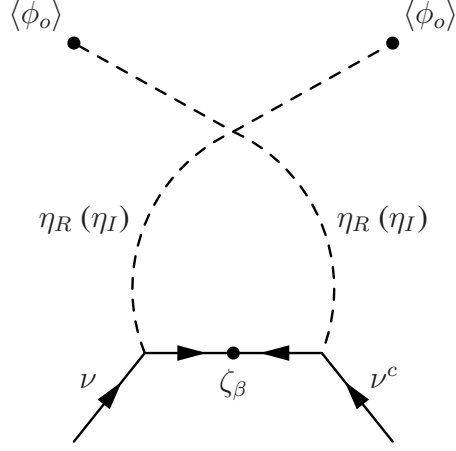


**Figure 1.** Radiative contributions for neutrino masses in the STSM. Notice that there are two contributions, one from  $\eta_R$  and other one from  $\eta_I$ .

number gets broken, the resulting effective neutrino mass matrix is given by:

$$\mathcal{M}_\nu^{\alpha\beta} = \sum_{\sigma=1}^2 \frac{h^{\alpha\sigma} h^{\beta\sigma}}{32\pi^2} m_{\zeta_\sigma} \left[ \frac{m_{\eta_R}^2 \ln \left( m_{\zeta_\sigma}^2 / m_{\eta_R}^2 \right)}{m_{\zeta_\sigma}^2 - m_{\eta_R}^2} - \frac{m_{\eta_I}^2 \ln \left( m_{\zeta_\sigma}^2 / m_{\eta_I}^2 \right)}{m_{\zeta_\sigma}^2 - m_{\eta_I}^2} \right], \quad (2.6)$$

where  $h_{\alpha\beta}$  ( $\alpha, \beta = 1, 2, 3$ ) are the Yukawa couplings in the matrix  $h$  introduced in Eq. (2.5),  $m_{\zeta_\sigma}$  ( $\sigma = 1, 2$ ) are the masses of the neutral fermions, and  $m_{\eta_{R,I}}$  are the masses of the fields  $\eta_R$  and  $\eta_I$  respectively. These become degenerate when the coupling  $\lambda''_{\phi\eta} \rightarrow 0$  signaling the lepton number conservation limit where neutrinos become massless.

As seen above, the structure of the coupling matrix  $h$  in Eq. (2.5) is also important for the phenomenology. If we had just one type of new fermions (either  $\Sigma$  or  $N$ ), let's say  $\Sigma$ , the structure of the matrix  $\mathcal{M}_\nu^{\alpha\beta}$  will be clearly projective

$$\mathcal{M}_\nu^{\alpha\beta} \propto \begin{bmatrix} Y_\Sigma^1 \\ Y_\Sigma^2 \\ Y_\Sigma^3 \end{bmatrix} [Y_\Sigma^1 \ Y_\Sigma^2 \ Y_\Sigma^3], \quad (2.7)$$

giving rise to only one nonzero eigenvalue, so that one can not explain neutrino oscillation data [4].

### 3 The Scalar Sector of the Model

#### 3.1 The Scalar Potential

We now turn our attention to the scalar sector of the model. As seen in table 1, the model includes a SM-like doublet  $\phi$  with hypercharge  $Y_\phi = 1/2$ , a doublet  $\eta$  with hypercharge

$Y_\eta = 1/2$  and odd  $\mathbb{Z}_2$  charge, and a triplet  $\Omega$  with hypercharge  $Y_\Omega = 0$  and even  $\mathbb{Z}_2$  charge, so that its neutral component can get a nonzero vev [16, 17]. Then, the scalar fields of this model are written as,

$$\phi = \begin{bmatrix} \phi^+ \\ \frac{v_\phi + \chi_\phi + i\varphi_\phi}{\sqrt{2}} \end{bmatrix}, \quad \eta = \begin{bmatrix} \eta^+ \\ \frac{\eta_R + i\eta_I}{\sqrt{2}} \end{bmatrix}, \quad \Omega = \begin{bmatrix} \frac{v_\Omega + \chi_\Omega}{\sqrt{2}} & \Omega^+ \\ \Omega^- & -\frac{v_\Omega + \chi_\Omega}{\sqrt{2}} \end{bmatrix} \quad (3.1)$$

Then, the corresponding scalar potential is given by,

$$\begin{aligned} V = & -m_\phi^2 \phi^\dagger \phi + m_\eta^2 \eta^\dagger \eta - \frac{1}{2} m_\Omega^2 \text{Tr}(\Omega^\dagger \Omega) + \frac{1}{2} \lambda_\phi (\phi^\dagger \phi)^2 + \frac{1}{2} \lambda_\eta (\eta^\dagger \eta)^2 + \frac{1}{4} \lambda_\Omega [\text{Tr}(\Omega^\dagger \Omega)]^2 \\ & + \lambda_{\phi\eta} (\phi^\dagger \phi) (\eta^\dagger \eta) + \lambda'_{\phi\eta} (\phi^\dagger \eta) (\eta^\dagger \phi) + \frac{1}{2} \lambda''_{\phi\eta} [(\phi^\dagger \eta)^2 + (\eta^\dagger \phi)^2] \\ & + \frac{1}{2} \lambda_{\phi\Omega} (\phi^\dagger \phi) \text{Tr}(\Omega^\dagger \Omega) + \frac{1}{2} \lambda_{\eta\Omega} (\eta^\dagger \eta) \text{Tr}(\Omega^\dagger \Omega) + \mu_{\phi\Omega} \phi^\dagger \Omega \phi + \mu_{\eta\Omega} \eta^\dagger \Omega \eta \end{aligned} \quad (3.2)$$

Where the mass square parameters  $m_\phi^2$ ,  $m_\eta^2$  and  $m_\Omega^2$  are all positive so that  $\eta$  is, in principle, unable to get a vev, so as to prevent breaking the  $\mathbb{Z}_2$  symmetry. The quartic couplings are chosen so that the low energy scalar potential is bounded from below. Those conditions are given by [17]

$$\lambda_\phi \geq 0, \quad \lambda_\eta \geq 0, \quad \lambda_\Omega \geq 0, \quad (3.3)$$

$$\lambda_{\phi\eta} + \sqrt{\lambda_\phi \lambda_\eta} \geq 0, \quad \lambda_{\phi\eta} + \lambda'_{\phi\eta} - |\lambda''_{\phi\eta}| + \sqrt{\lambda_\phi \lambda_\eta} \geq 0, \quad (3.4)$$

$$\lambda_{\phi\Omega} + \sqrt{2\lambda_\phi \lambda_\Omega} \geq 0, \quad \lambda_{\eta\Omega} + \sqrt{2\lambda_\eta \lambda_\Omega} \geq 0 \quad (3.5)$$

$$\begin{aligned} & \sqrt{2\lambda_\phi \lambda_\eta \lambda_\Omega} + \lambda_{\phi\eta} \sqrt{2\lambda_\Omega} + \lambda_{\phi\Omega} \sqrt{\lambda_\eta} \\ & + \lambda_{\eta\Omega} \sqrt{\lambda_\phi} + \sqrt{(\lambda_{\phi\eta} + \sqrt{\lambda_\phi \lambda_\eta}) (\lambda_{\phi\Omega} + \sqrt{2\lambda_\phi \lambda_\Omega}) (\lambda_{\eta\Omega} + \sqrt{2\lambda_\eta \lambda_\Omega})} \geq 0. \end{aligned} \quad (3.6)$$

These were obtained after using copositivity conditions [18] inside the scalar potential. As shown in [17], even if one starts from an adequately consistent potential at the electroweak scale, one could reach a situation in which the Lagrangian is no longer invariant under the  $\mathbb{Z}_2$  symmetry at high energies, signalling that this symmetry could be broken, i.e.  $m_\eta^2 < 0$ .

This problem can be avoided, in general, by choosing a not too large value for the mass parameter  $\mu_{\eta\Omega}$ , namely, in the order of  $\lesssim$  TeV. We stress that this is just a reasonable prescription and not a full solution. While a more involved scan in this direction would be required, it lies out of the scope of the present work (see [17] for further details).

### 3.2 The Scalar Mass Spectrum

First we notice that after electroweak symmetry breaking, the  $\eta$  field has no mixings with other fields, thus the physical masses in this  $\mathbb{Z}_2$ -odd sector are given by

$$m_{\eta^R}^2 = m_\eta^2 + \frac{1}{2}(\lambda_{\phi\eta} + \lambda'_{\phi\eta} + \lambda''_{\phi\eta})v_\phi^2 + \frac{1}{2}\lambda_{\eta\Omega}v_\Omega^2 - \frac{1}{\sqrt{2}}\mu_{\eta\Omega}v_\Omega \quad (3.7)$$

$$m_{\eta^I}^2 = m_\eta^2 + \frac{1}{2}(\lambda_{\phi\eta} + \lambda'_{\phi\eta} - \lambda''_{\phi\eta})v_\phi^2 + \frac{1}{2}\lambda_{\eta\Omega}v_\Omega^2 - \frac{1}{\sqrt{2}}\mu_{\eta\Omega}v_\Omega \quad (3.8)$$

$$m_{\eta^+}^2 = m_\eta^2 + \frac{1}{2}\lambda_{\phi\eta}v_\phi^2 + \frac{1}{2}\lambda_{\eta\Omega}v_\Omega^2 + \frac{1}{\sqrt{2}}\mu_{\eta\Omega}v_\Omega \quad (3.9)$$

Turning to the pseudoscalar  $\mathbb{Z}_2$ -even sector, it is given just by  $\varphi_\phi$  (the imaginary part of the neutral component of the Higgs doublet  $\phi$  in eq. (3.1)), and does not contain terms from  $\eta$  (because it has no vev) or  $\Omega$  (because it has no hypercharge). This means that  $\Omega^0$  is real, so that the  $Z$  boson receives a longitudinal component just from the Higgs-like doublet and not from the triplet.

Something different happens in the charged  $\mathbb{Z}_2$ -even sector, since the charged component of the triplet  $\Omega$  does mix with the charged component of the Higgs doublet  $\phi^+$ . Hence the  $W$  boson longitudinal mode is a linear combination of  $\phi^+$  and  $\Omega^+$ . After solving the tadpole equations for the squared mass parameters  $m_\phi^2$  and  $m_\Omega^2$ , we obtain the charged scalar squared mass matrix in the basis  $(\phi^+, \Omega^+)^T$  as:

$$M_+^2 = \frac{1}{2\sqrt{2}} \frac{\mu_{\phi\Omega}}{v_\Omega} \begin{bmatrix} 4v_\Omega^2 & 2v_\phi v_\Omega \\ 2v_\phi v_\Omega & v_\phi^2 \end{bmatrix} \quad (3.10)$$

The diagonalization of this mass matrix is performed as  $O_c M_+^2 O_c^T = \text{diag}(m_{G^\pm}^2, m_{H^\pm}^2)$ , where the orthogonal matrix  $O_c$  is

$$O_c = \begin{bmatrix} c_\beta & -s_\beta \\ s_\beta & c_\beta \end{bmatrix} \quad (3.11)$$

where the mixing angle is given as

$$c_\beta = \frac{v_\phi}{\sqrt{v_\phi^2 + 4v_\Omega^2}}, \quad s_\beta = \frac{2v_\Omega}{\sqrt{v_\phi^2 + 4v_\Omega^2}} \quad (3.12)$$

In this case, the masses eigenvalues are

$$\begin{aligned} m_{G^\pm}^2 &= 0 \\ m_{H^\pm}^2 &= \frac{1}{2\sqrt{2}} \frac{\mu_{\phi\Omega}}{v_\Omega} (v_\phi^2 + 4v_\Omega^2) \end{aligned} \quad (3.13)$$



Here the zero mass eigenstate corresponds to the charged Goldstone boson and the massive eigenstate corresponds to a physical charged scalar. Since the  $\rho$  parameter receives contributions from the vev  $v_\Omega$ , having  $\rho = 1$  constrains the vev of the triplet to be much smaller than the Higgs-doublet vev (the limit is set to  $v_\Omega \lesssim 5$  GeV). This implies that the Goldstone boson is mainly doublet, while the massive charged scalar is mainly triplet. Therefore, we can make the following approximation for charged scalar mass,

$$m_{H^\pm}^2 \approx \frac{1}{2\sqrt{2}} \frac{\mu_{\phi\Omega}}{v_\Omega} v_\phi^2 \quad (3.14)$$

One sees that by taking  $\mu_{\phi\Omega} > v_\Omega$  one can have a charged Higgs in agreement with current experiments. In order to find the mass eigenstates for the neutral scalar mass matrix, we follow a similar procedure. After solving the tadpoles for  $m_\phi^2$  and  $m_\Omega^2$ , the CP-even Higgs mass matrix in the basis  $(\chi_\phi, \chi_\Omega)^T$  becomes,

$$M_\chi^2 = \begin{bmatrix} \lambda_\phi v_\phi^2 & \lambda_{\phi\Omega} v_\phi v_\Omega - \frac{1}{\sqrt{2}} \mu_{\phi\Omega} v_\phi \\ \lambda_{\phi\Omega} v_\phi v_\Omega - \frac{1}{\sqrt{2}} \mu_{\phi\Omega} v_\phi & 2\lambda_\Omega v_\Omega^2 + \frac{1}{2\sqrt{2}} \mu_{\phi\Omega} \frac{v_\phi^2}{v_\Omega} \end{bmatrix} \quad (3.15)$$

In this case we have two massive eigenstates. The lightest one is identified with the Higgs of 125 GeV, while the second one will be our heavy Higgs and the center of our following analysis. This is motivated by negative searches for a light Higgs boson [19, 20, 21]. We define  $\alpha$  as the mixing angle in the CP-even sector, which defines the following orthogonal matrix:

$$O_\chi = \begin{bmatrix} c_\alpha & -s_\alpha \\ s_\alpha & c_\alpha \end{bmatrix} \quad (3.16)$$

such that  $O_\chi M_\chi^2 O_\chi^T = \text{diag}(m_{h_1}^2, m_{h_2}^2)$ , with the mass eigenstates named  $h_1$  and  $h_2$  in increasing mass ordering. Notice that we want that the first eigenstate to be Higgs-like in order to agree with the experiments, which force  $c_\alpha$  to be larger than  $s_\alpha$ . In this setup, it is immediate that the second neutral state  $h_2$  will be mainly triplet.

By using again the approximation in which  $v_\phi \gg v_\Omega$ , and  $\mu_{\phi\Omega} > v_\Omega$ , the eigenvalues of the neutral CP-even mass matrix can be greatly simplified to:

$$\begin{aligned} m_{h_1}^2 &\approx \lambda_\phi v_\phi^2 \\ m_{h_2}^2 &\approx \frac{1}{2\sqrt{2}} \frac{\mu_{\phi\Omega}}{v_\Omega} v_\phi^2 \approx m_{H^\pm}^2 \end{aligned} \quad (3.17)$$

So that, this setting always admits a light doublet-like Higgs ( $h_1$ ) and a heavy triplet-like Higgs ( $h_2$ ), in which the heavy Higgses are nearly degenerate, so that  $m_{h_2}^2 \approx \frac{1}{2\sqrt{2}} \frac{\mu_{\phi\Omega}}{v_\Omega} v_\phi^2 \approx m_{H^\pm}^2$ .

## 4 Numerical Analysis

### 4.1 Parameter Space

We now turn to the description of the physically acceptable parameter space of the model. We vary randomly the values of the different parameters, but requiring: boundedness from below of the scalar potential, and the exact conservation of the  $\mathbb{Z}_2$  symmetry, as already been discussed above. Moreover we require that the lightest Higgs bosons with 125 GeV mass is mainly doublet by demanding  $|O_\chi^{11}| > 0.9$  which is satisfied by most of our generated scenarios. With these restrictions we seek to obtain consistent neutrino physics (Sec.4.1.1 below) and a correct dark matter relic abundance with a scalar dark matter candidate, Sec. 4.1.2 below. Recall that, as we stated in the end of the section 2.1, we will pick the  $\eta_R$  as the dark matter candidate of our model.

#### 4.1.1 Neutrino mass

In our study of scotogenic dark matter we need first to implement the neutrino oscillation constraints. As usual, this can be achieved in two configurations which are called normal and inverse mass orderings. A feature of our singlet-triplet scotogenic model is that one of the neutrinos is massless, simplifying the discussion. For further convenience, we use the Casas-Ibarra parametrization [22]. Since our results do not depend on the detailed nature of the neutrino spectrum, we also choose to focus on the case of normal ordering for neutrino masses. This can be understood since neither dark matter nor the collider phenomenology are sensitive to the individual masses of different neutrino species, and hence to their specific mass hierarchy [24]. Small values of  $\lambda''_{\phi\eta}$  were chosen by the original references [16, 17] in order to have small neutrino masses with  $\mathcal{O}(1)$  Yukawa couplings<sup>2</sup>. This fits with t’Hooft naturalness principle, since making  $\lambda''_{\phi\eta}$  zero would deliver a Lagrangian with an extra  $U(1)$  symmetry which is identified with lepton number. Here we allow  $\lambda''_{\phi\eta}$  to take on larger values. This implies the need for choosing small values for the Yukawa couplings so as to account for small neutrino masses [24]. Moreover it implies that the degeneracy between  $m_{\eta_R}$  and  $m_{\eta_I}$  is lifted.

In Fig. 2 we show a general scatter plot (all model parameters are randomly varied) for points in parameter space that satisfy the measured neutrino oscillation parameters and other constraints. It shows the Yukawa coupling  $|Y_N^1|$  as a function of  $|\lambda''_{\phi\eta}|$ . One sees that a large Yukawa coupling requires a small value for  $|\lambda''_{\phi\eta}|$  and vice-versa. A similar behavior is observed in the other Yukawa couplings, in fact, since neutrino masses have well defined values, there is a correlation between the Yukawas (encoded in the matrix  $h$ ) and  $\lambda''_{\phi\eta}$ . In the

---

<sup>2</sup>In references [16, 17] the parameter  $\lambda''_{\phi\eta}$  is named  $\lambda_5$ .

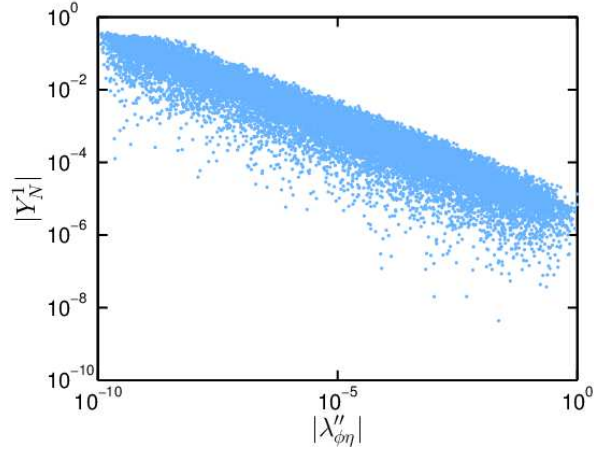


**Figure 2.** Scan where all the independent parameters of the model are varied. The absolute value  $|Y_N^1|$  of one of the Yukawa couplings is presented as a function of  $|\lambda''_{\phi\eta}|$ . It shows that  $|\lambda''_{\phi\eta}|$  can be large as long as the Yukawa couplings are small.

limit where  $\lambda''_{\phi\eta} v_\phi^2 \ll m_0^2$ ,  $m_{\zeta_\sigma}^2$  and  $\lambda''_{\phi\eta} v_\phi^2 \ll m_0^2 - m_{\zeta_\sigma}^2$ , we find that

$$\mathcal{M}_\nu^{\alpha\beta} = \sum_{\sigma=1}^2 \frac{h^{\alpha\sigma} h^{\beta\sigma}}{32\pi^2} m_{\zeta_\sigma} \frac{\lambda''_{\phi\eta} v_\phi^2}{m_{\zeta_\sigma}^2 - m_0^2} \mathcal{F}(m_{\zeta_\sigma}, m_0) \quad (4.1)$$

Where the function  $\mathcal{F}$  involves only logarithms of the quantities  $m_{\zeta_\sigma}$  and  $m_0$ , and in turn (c.f. Eqs. (3.7) and Eqs. (3.8)):

$$m_0^2 \equiv m_\eta^2 + \frac{1}{2}(\lambda_{\phi\eta} + \lambda'_{\phi\eta})v_\phi^2 + \frac{1}{2}\lambda_{\eta\Omega} v_\Omega^2 - \frac{1}{\sqrt{2}}\mu_{\eta\Omega} v_\Omega \quad (4.2)$$

Actually, the correlation between  $Y_{N,\Sigma}$  and  $\lambda''_{\phi\eta}$  is general and shows up basically in any limits that one may take in eq. (2.6) [29].

#### 4.1.2 Relic density

Due to the presence of the  $Z_2$  symmetry we have three possible dark matter candidates in our model:  $\eta_R$ ,  $\eta_I$ , see eq. (3.1) or  $\zeta_1$ , see eq. (2.4). The lightest of these states is a potential WIMP DM candidate within our scotogenic scenario. For example, the possibility of the fermion  $\zeta_1$  being the dark matter candidate has been studied before [16]. For definiteness, in our following analysis we assume the alternative possibility that the DM is the  $\eta_R$  field and study its viability.

In Fig. 3 we show a plot of the dark matter relic abundance as a function of the mass of the scalar dark matter candidate, which is taken to be  $\eta_R$ . Only points obeying  $|c_\alpha| \equiv |O_X^{11}| >$

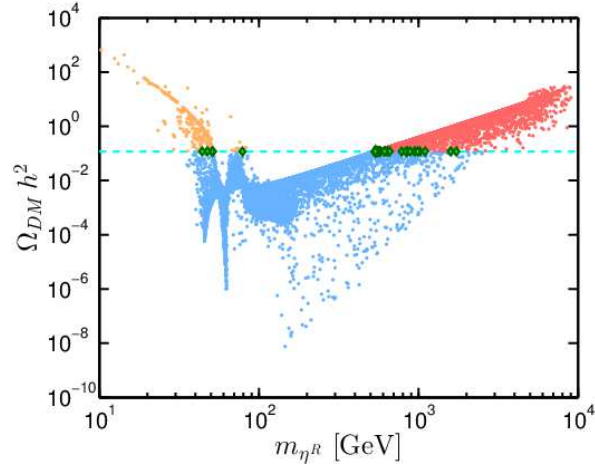


**Figure 3.** Relic density for our dark matter candidate  $\eta_R$  as a function of its mass. We show a scan varying all the independent parameters of the model. Only points with  $h_1$  mainly doublet are displayed. See the text for the color code.

0.9 are shown, because experimental results seem to prefer a SM-like 125 GeV Higgs boson [25]. The measured value for the relic abundance lies in a small region which is shown as a cyan horizontal line in the figure [26, 27]. The color code for the points is explained as follows. Points that fulfill the measured value of the relic density are painted in green. In blue, we have points that have a relic abundance under the  $3\sigma$  region on the current measurements; the red and orange ones have a relic abundance over the mentioned region. Nevertheless, the blue points are only ruled out if we consider the  $\eta_R$  as the only source of Dark Matter. Notice that this model has similar results for direct dark matter detection to those of the IHDM model. In fact, one sees two dips in the relic abundance plot in fig. 3, which correspond to the situations where the DM has resonant scattering through a Higgs or Z boson at  $\sim 45$  GeV and  $\sim 62.5$  GeV. The same features are also present in IHDM case [30]. Concerning the phenomenology of dark matter in this model it is worth mentioning that scalar dark matter can be detected directly by nuclear recoil through the Higgs portal mechanism, as well as at the LHC and indirectly [10, 28, 29, 30, 31]. For instance the mass gap that separates red and orange points in the present model has its analogous gap in that case too. This is not surprising since both models share many features. The difference  $m_{\eta_I} - m_{\eta_R}$  is intimately connected with the violation of lepton number and the value of  $\lambda''_{\phi\eta}$ , as it can be seen from equations (3.7) and (3.8). In fact, by taking the limit of small  $\lambda''_{\phi\eta}$  in these equations one finds

$$m_{\eta_R} - m_{\eta_I} \approx \frac{2\lambda''_{\phi\eta} v_\phi^2}{\sqrt{3}m_0}. \quad (4.3)$$

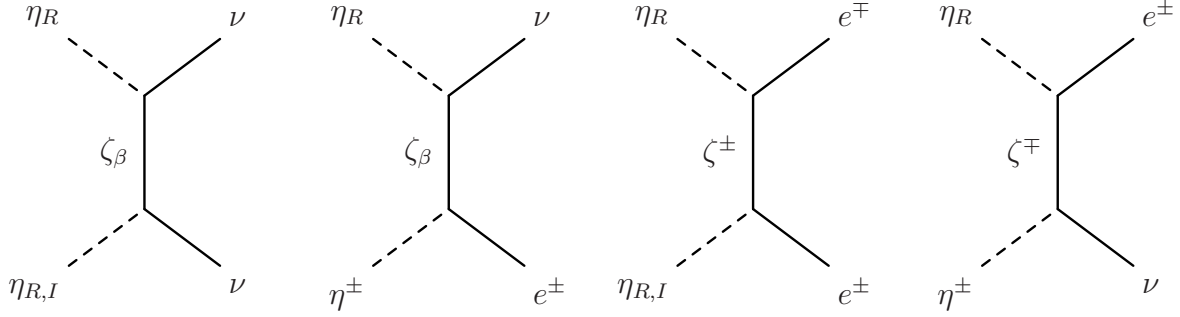


**Figure 4.** Illustrative Feynman diagrams for scalar annihilation/coannihilation channels involving Yukawa couplings  $Y_N$  and  $Y_\Sigma$ .

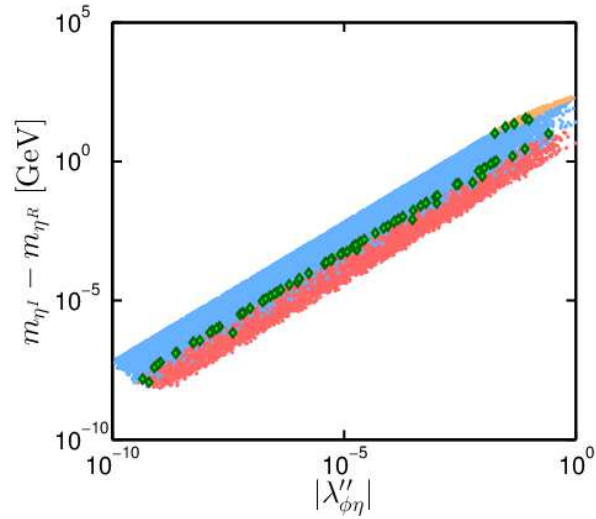


**Figure 5.** Mass difference  $m_{\eta_I} - m_{\eta_R}$  as a function of  $|\lambda''_{\phi\eta}|$  with identical color code as in the previous figure. Interesting is to notice that low values of  $m_{\eta_R}$  with an excess of relic density are associated to high values of  $|\lambda''_{\phi\eta}|$ .

This implies a relation between dark matter relic abundance and neutrino physics, since the Yukawas  $Y_\Sigma$  and  $Y_N$  are involved both in the neutrino mass generation as in the DM annihilation cross section. For instance, the annihilation  $\eta_R\eta_R \rightarrow \nu\nu$  can be seen from the Lagrangian 2.1, in which the Yukawa couplings  $Y_N$  and  $Y_\Sigma$  indicate interactions among the DM candidate, neutrinos and the neutral fermions  $\Sigma_0$  and  $N$ , so that they lead to a t-channel contribution to the annihilation cross section. Scalar annihilation/coannihilation channels generated by the Yukawa couplings  $Y_N$  and  $Y_\Sigma$  are shown in Fig. 4.

In Fig. 5 we see the mass difference  $m_{\eta_I} - m_{\eta_R}$  as a function of  $|\lambda''_{\phi\eta}|$ , with the same

color code as in the previous figure. We notice that the orange points, associated to large values of  $|\lambda''_{\phi\eta}|$  in Fig. 5 are also associated to the small values of the dark matter mass in Fig. 3. Therefore, small values for  $m_{\eta_R}$  (DM) need very small Yukawa couplings,  $Y_N$  and  $Y_\Sigma$ , reason why we consider them disfavored. Notice also that many points that give the correct relic density lie in the whole range for  $|\lambda''_{\phi\eta}|$ , approximately at the intersection of the blue and red regions. Notice also that eq.(4.3) shows that there are two ways to enforce the degeneracy between  $\eta_R$  and  $\eta_I$  fields. One of them is the smallness of  $|\lambda''_{\phi\eta}|$ , and the other the largeness of  $m_0$ . This degeneracy is important because it determines the smallness of neutrino mass. Unfortunately, however, it is not directly translated into a prediction for the relic abundance. Indeed, all the blue and red points correspond to degeneracy, while the orange ones do not.

## 4.2 Production of heavy Higgs boson

### 4.2.1 Two benchmark points

In this section we study the phenomenology of the heavy neutral Higgs boson  $h_2$  present in this model. We choose two different benchmarks, that we call B1 and B2. They are required to be consistent with a scalar DM candidate and the other constraints described above. B1 is given in Table 2 and the corresponding scalar spectrum is given in Table 3. In order to obtain a lighter Higgs boson spectrum, so as to study the branching ratios and LHC production cross sections, we define B2 by starting from B1 and changing only one parameter. This parameter is chosen to be  $\mu_{\phi\Omega}$ , since it controls the masses of  $H^+$  and  $h_2$ , as shown in eqs. (3.14) and (3.17). We vary it from  $\mu_{\phi\Omega} = 54$  GeV in B1 to  $\mu_{\phi\Omega} = 11$  GeV in B2. This change produces a lighter spectrum in B2 as compared to B1, as seen in Table 3. Other possible benchmark points hardly affect the cross sections of interest to us, except that of the two largest cross sections (see fig. 6),  $\sigma(e^+e^- \rightarrow h_2 H^\pm W^\mp)$  rises with the parameter  $v_\Omega$ , while  $\sigma(e^+e^- \rightarrow h_2 \nu_i \bar{\nu}_j)$  is unaffected. Therefore, since we know the effect of varying  $v_\Omega$ , we did not include a benchmark with a smaller  $v_\Omega$ .

The neutrino sector is unchanged, and the same Yukawa couplings are chosen in both benchmarks in order to satisfy neutrino mass square differences and mixing angles required in order to account for neutrino oscillation data [4]. The Yukawa couplings are also given in the table. The scalar spectra in both benchmarks is given in table 3. The particles  $h_2$  and  $H^+$  are both mainly triplet, and as a result their masses are similar irrespective of the benchmark (in B1  $H^+$  is 6 MeV lighter than  $h_2$ ). As mentioned before,  $\eta_R$  and  $\eta_I$  have a very similar mass too, and this is related to the symmetry that dictates the smallness of the neutrino masses.

In both benchmarks  $\eta_I$  is around 80 MeV heavier than  $\eta_R$  (our dark matter particle). Thus, the largest difference between the two benchmarks is that the new scalars are relatively

Parameter	Benchmark 1	Benchmark 2	Units
$v_\phi$	246	246	GeV
$v_\Omega$	3.7	3.7	GeV
$\lambda_\phi$	0.263	0.263	-
$\lambda_\eta$	0.41	0.41	-
$\lambda_\Omega$	0.65	0.65	-
$\lambda_{\phi\eta}$	0.75	0.75	-
$\lambda'_{\phi\eta}$	-0.86	-0.86	-
$\lambda''_{\phi\eta}$	-0.0041	-0.0041	-
$\lambda_{\phi\Omega}$	0.47	0.47	-
$\lambda_{\eta\Omega}$	0.82	0.82	-
$\mu_{\phi\Omega}$	54	11	GeV
$\mu_{\eta\Omega}$	910	910	GeV
$ m_\eta $	1690	1690	GeV
$Y_\Omega$	$-2.7 \times 10^{-1}$	$-2.7 \times 10^{-1}$	-
$Y_N^1$	$1.1 \times 10^{-4}$	$1.1 \times 10^{-4}$	-
$Y_N^2$	$1.0 \times 10^{-4}$	$1.0 \times 10^{-4}$	-
$Y_N^3$	$-1.3 \times 10^{-4}$	$-1.3 \times 10^{-4}$	-
$Y_\Sigma^1$	$-1.0 \times 10^{-4}$	$-1.0 \times 10^{-4}$	-
$Y_\Sigma^2$	$-5.0 \times 10^{-4}$	$-5.0 \times 10^{-4}$	-
$Y_\Sigma^3$	$-4.4 \times 10^{-4}$	$-4.4 \times 10^{-4}$	-

**Table 2.** Independent parameters for the benchmark, relevant for the scalar sector, including dark matter (above), and the Yukawa sector (below).

Parameter	Benchmark 1	Benchmark 2
$m_{h_1}$	125	125
$m_{h_2}$	560	253
$m_{H^+}$	560	252
$m_{\eta^R}$	1688	1688
$m_{\eta^I}$	1688	1688
$m_{\eta^+}$	1697	1697

**Table 3.** Scalar physical masses in GeV for the chosen benchmarks.

heavier in B1.

Using the latest version of Madgraph [32] we calculate the  $h_2$  production cross sections

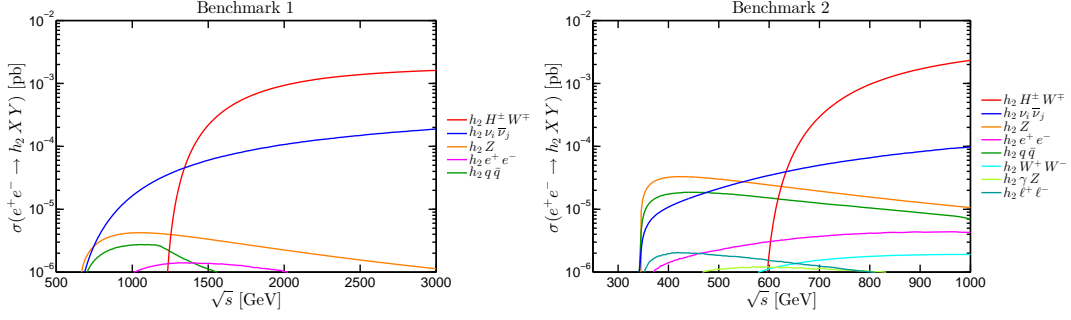


**Figure 6.** Two and three body production cross section for  $h_2$  in an electron-positron collider as a function of  $\sqrt{s}$  for both benchmarks.

for both benchmarks. The results are displayed in Fig. 6. There we give 2-body and 3-body production cross sections as a function of the center of mass energy (c.m.)  $\sqrt{s}$  in an electron-positron collider. To evaluate the reach of a couple of planned electron-positron colliders we mention that the projected c.m. energies and luminosities for the International Linear Collider (ILC) are 250 GeV, 500 GeV, and 1000 GeV, with  $250 \text{ fb}^{-1}$ ,  $500 \text{ fb}^{-1}$ , and  $1000 \text{ fb}^{-1}$  respectively [33]. For the case of the Compact Linear Collider (CLIC) these are  $\sqrt{s} = 350 \text{ GeV}$ , 1.4 TeV, and 3 TeV, with estimated luminosities  $500 \text{ fb}^{-1}$ ,  $1.5 \text{ ab}^{-1}$ , and  $2 \text{ ab}^{-1}$  respectively [34].

We see in Fig. 6 that the only relevant 2-body  $h_2$  production mechanism is  $e^+ e^- \rightarrow h_2 Z$ , which is suppressed up to 3 orders of magnitude at  $\sqrt{s} = 3 \text{ TeV}$  for B1, and suppressed up to 2 orders of magnitude at  $\sqrt{s} = 1 \text{ TeV}$  for B2, compared to the main 3-body production mode at those energies. The channel  $e^+ e^- \rightarrow h_2 Z$  can dominate at low energies though, as can be seen in the B2 frame. Concerning 3-body production modes, the largest two are  $e^+ e^- \rightarrow h_2 H^\pm W^\mp$  (including a factor of 2 due to the choice of electric charge) and  $e^+ e^- \rightarrow h_2 \nu_i \bar{\nu}_j$  in both benchmarks. The production process  $e^+ e^- \rightarrow h_2 H^+ W^-$  is in turn dominated by the sub-process where a neutrino is in the t-channel and a  $W$  boson produces the pair  $h_2 H^+$ . Thus, the coupling  $h_2 H^+ W^-$  becomes important. Since  $h_2$  and  $H^+$  are mainly triplet, this coupling is not suppressed with respect to the gauge coupling. The 3-body production mode  $e^+ e^- \rightarrow h_2 \nu_i \bar{\nu}_j$  is one of the two known as ‘‘Vector Boson Fusion’’ (VBF), because the mentioned process is dominated by a sub-process where a  $W$  boson is emitted from the electron (and positron) and they ‘‘fuse’’ to create an  $h_2$ . If we replace the  $W$  boson by a  $Z$  boson we find the second VBF process  $e^+ e^- \rightarrow h_2 e^+ e^-$ . It is worth mentioning that this last VBF is suppressed with respect to  $e^+ e^- \rightarrow h_2 \nu_i \bar{\nu}_j$ , as can be seen in Fig. 6, because most of the charged leptons go through the beam pipe. If we use the corresponding cut (Madgraph has this cut by default), the cross section diminishes considerably



[35]. As with the 2-body production mode,  $e^+ e^- \rightarrow h_2 \nu_i \bar{\nu}_j$  can be the dominant process at low energies. We also note the reader that we have checked that when we decrease the triplet vev  $v_\Omega$  the cross section  $\sigma(e^+ e^- \rightarrow h_2 H^+ W^-)$  is hardly affected while the cross section  $\sigma(e^+ e^- \rightarrow h_2 \nu_i \bar{\nu}_j)$  decreases, as expected from the couplings involved.

If we naively compare the production cross sections shown in Fig. 6 with the projected luminosities of ILC and CLIC given in the immediately following paragraph we conclude that ILC will have the chance to observe  $h_2$  in this model only if its mass is low (as given in B2). On the contrary, CLIC will have enough energy and luminosity to observe  $h_2$  in both benchmarks [35].

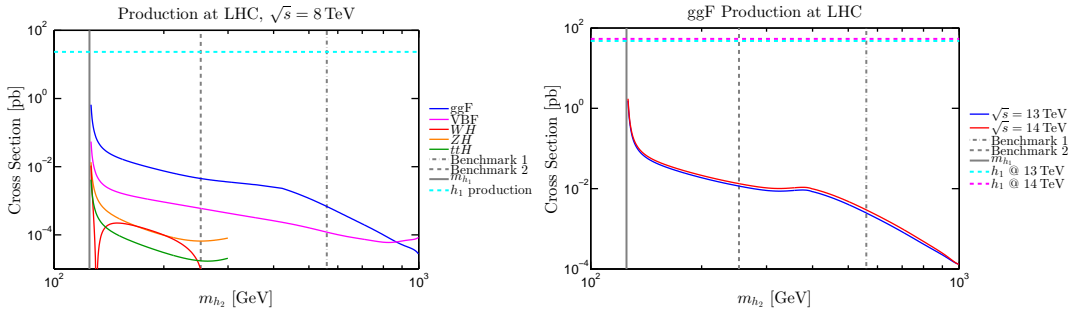


**Figure 7.** Cross section at the LHC. The vertical grey dashed lines correspond to the value of  $m_{h_2}$  in our benchmarks. The left panel shows the cross sections computed for  $\sqrt{s} = 8$  TeV and the right panel is for  $\sqrt{s} = 13$  and 14 TeV.

We argue that it will be very difficult to observe  $h_2$  at the LHC. In Fig. 7 we see the production cross section at the LHC for  $h_2$  as a function of its mass. In the left frame we have it for the center of mass energy  $\sqrt{s} = 8$  TeV, and in the right frame we have it for 13 and 14 TeV c.m. energy. In both cases we have the gluon-gluon fusion (ggF) production mode, while for the low energy (8 TeV) we have also other less important production modes. The two vertical dashed lines indicate the value of  $m_{h_2}$  in both benchmarks, and for reference we also show in a vertical solid line the value of the SM-like Higgs 125 GeV. The horizontal dashed lines indicates the value of the LHC production cross section of a 125 GeV SM-like Higgs boson.

The main message of Fig. 7 is that independently of the c.m. energy, the production cross section of  $h_2$  at the LHC is 3 to 5 orders of magnitude (depending on  $m_{h_2}$ ) smaller than the production cross section of the SM-like Higgs boson. The principal reason for this behaviour is that the ggF production mode is based on the  $h_2$  coupling to quarks. Since only the Higgs doublet couple to fermions, and since  $h_2$  is mainly triplet, that coupling is highly

suppressed. Therefore, any hadron collider that relies on ggF for the production of the scalar will have a hard time to observe  $h_2$ .

#### 4.2.2 Decay Rates for the Charged and Heavy CP-Even Higgs

In this section we calculate the decay rates for  $h_2$  and  $H^+$  using the latest version of SPheno code [36], where our model is implemented. In Fig. 8 we have the 2-body decay modes for

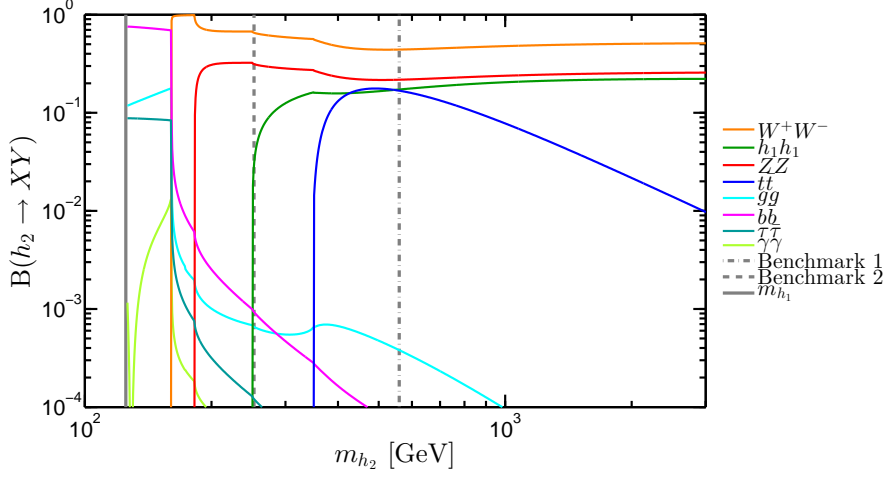


**Figure 8.** Branching ratios for  $h_2$  as a function of its mass. When the channels are open, the main decay modes are  $h_2 \rightarrow WW$  and  $h_2 \rightarrow ZZ$ .

$h_2$  as a function of its mass. The solid, dashed, and dot-dashed vertical lines indicate the 125 GeV mass for the SM-like Higgs boson, and the value for  $m_{h_2}$  in our two benchmarks. We create each branching ratio line varying only one parameter,  $\mu_{\phi\Omega}$ . Thus, at the intersection with the corresponding vertical line, we sit exactly at each of the two benchmarks.

Above the  $ZZ$  threshold, the dominant decay mode is  $h_2 \rightarrow WW$  followed by  $h_2 \rightarrow ZZ$ . The first decay follows because the Higgs  $h_2$  is mostly triplet and has interactions with two  $W$  bosons via the Higgs kinetic term in the Lagrangian. The decay rate for  $h_2 \rightarrow ZZ$  is penalized because the triplet has null hypercharge and only couples to two  $Z$  bosons through the  $h_2$  component to doublet. The third important decay mode is  $h_2 \rightarrow h_1h_1$ . This decay mode is important because we have chosen a large value for  $\mu_{\phi\Omega}$ . In addition,  $\lambda_{\phi\Omega}$  is large, although its contribution is proportional to the (small) triplet vev  $v_\Omega$ . The enhancement of the decay  $h_2 \rightarrow t\bar{t}$ , which also proceeds via the  $h_2$  component to doublet, and is given by the contribution of (large) Yukawa coupling. Finally, the similar behavior of the channels involving gauge bosons in the final state and the channel with two light Higgs relies on a proportionality of  $m_{h_2}^3$  of the three channels, being the coupling  $O_{h_2h_1h_1}$  proportional to  $\mu_{\phi\Omega}$  which in turn is proportional to  $m_{h_2}$  (see eqs. (A.1) and (A.3)).

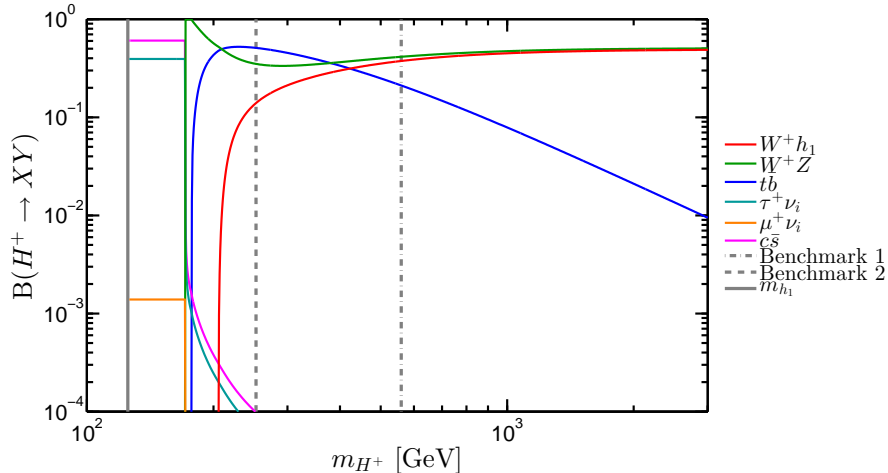


**Figure 9.** Branching ratios for  $H^+$  as a function of its mass. When the channels are open, the main decay modes are  $H^+ \rightarrow W^+Z$ ,  $H^+ \rightarrow t\bar{b}$ , and  $H^+ \rightarrow W^+h_1$ .

In Fig. 9 we show the decay channels for the charged Higgs boson as a function of its mass following the same technique described earlier for the previous case. We are interested in the decay modes of the charged Higgs because production cross sections for  $h_2$  are enhanced when it is accompanied by a charged Higgs, as can be appreciated in Fig. 6. Above the  $t\bar{b}$  threshold, three decay modes take turns in being the dominant one:  $H^+ \rightarrow ZW^+$ ,  $H^+ \rightarrow t\bar{b}$ , and  $H^+ \rightarrow h_1W^+$ . From the coupling point of view, all three decay rates are small, but this is not necessarily reflected in branching ratios. the coupling  $H^+ZW^-$  is proportional to the triplet vev, the coupling  $H^+t\bar{b}$  is proportional to the  $H^+$  component to doublet, and the coupling  $H^+h_1W^-$  is small because  $H^+$  is mostly triplet while  $h_1$  is mostly doublet. In the same way as the channels for a heavy neutral Higgs, the decay modes of the charged Higgs going to  $W^+h_1$  and  $W^+Z$  behave as  $m_{H^+}^3$  at large masses of this field, as it can be concluded from eqs (A.7) and (A.8).

## 5 Conclusions

We have considered the proposal that the dark matter particle is a scalar WIMP messenger associated to neutrino mass generation, whose stability follows from the same symmetry responsible for the radiative origin of neutrino mass. This hypothesis embodies a simple model for WIMP dark matter and provides a useful benchmark for electroweak symmetry breaking studies at accelerators. This picture was illustrated within the singlet-triplet scotogenic dark matter model. We have studied in detail the symmetry breaking sector of this model and the corresponding pattern of WIMP interactions, showing how it can provide adequate neu-

trino masses and dark matter relic density. We have characterized the expected profile of heavy Higgs boson physics as expected at the LHC and at future linear Colliders. Our study constitutes a first step towards a comprehensive approach to the idea that WIMP dark matter emerges as a messenger connected to neutrino mass generation, which should encourage dedicated simulations of the associated signatures.

## Acknowledgments

This work was partly funded by the Spanish grants FPA2014-58183-P, Multidark CSD2009-00064, SEV-2014-0398 (MINECO) and PROMETEOII/2014/084 (Generalitat Valenciana). MAD was partly funded by the Fondecyt Grant 1141190. NR was funded by becas de postdoctorado en el extranjero Conicyt/Becas Chile (2015) 74150028.

## A Appendix : Feynman Rules for Decay Channels

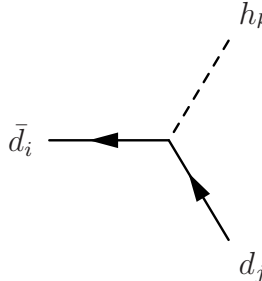
In this section we list some of the Feynman rules of the model relevant to evaluate the decays used in this paper. For generality intergenerational mixing was included, though not strictly necessary for this paper. Throughout these diagrams, all the momenta are incoming.

### A.1 Diagrams Involving Neutral Higgses

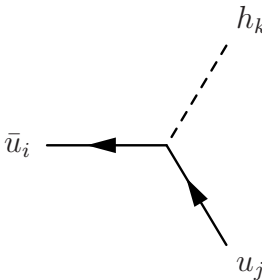
$$\begin{aligned}
 & \begin{array}{c} W_{\mu}^{+} \\ \text{---} \\ h_i \text{ ---} \\ \text{---} \\ W_{\sigma}^{-} \end{array} = iO_{h_i WW} g_{\sigma\mu} \\
 & = \frac{i}{2} g_{\sigma\mu} g_2^2 (4v_{\Omega} O_{\chi}^{i2} + v_{\phi} O_{\chi}^{i1}) \quad (A.1)
 \end{aligned}$$

$$\begin{aligned}
& \text{Diagram: } h_i \text{ (dashed) } \rightarrow \begin{cases} Z_\mu \text{ (wavy)} \\ Z_\sigma \text{ (wavy)} \end{cases} \\
& = iO_{h_i ZZ} g_{\sigma\mu} \\
& = \frac{i}{2} g_{\sigma\mu} v_\phi O_\chi^{i1*} (g_1 \sin \Theta_W + g_2 \cos \Theta_W)^2 \quad (\text{A.2})
\end{aligned}$$

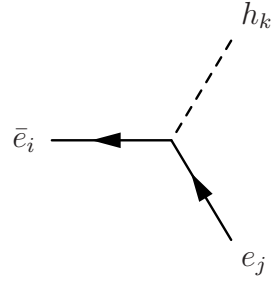
$$\begin{aligned}
& \text{Diagram: } h_i \text{ (dashed) } \rightarrow \begin{cases} h_k \text{ (dashed)} \\ h_j \text{ (dashed)} \end{cases} \\
& = ig_{h_i h_j h_k} \\
& = \frac{i}{2} \left\{ O_\chi^{i2} \left[ -2O_\chi^{j2} (6\lambda_{\phi\Omega} v_\Omega O_\chi^{k2} + \lambda_{\phi\Omega} v_\phi O_\chi^{k1}) \right. \right. \\
& \quad + O_\chi^{j1} \left\{ (-2\lambda_{\phi\Omega} v_\Omega + \sqrt{2}\mu_{\phi\Omega}) O_\chi^{k1} - 2\lambda_{\phi\Omega} v_\phi O_\chi^{k2} \right\} \left. \right] \\
& \quad + O_\chi^{i1} \left[ O_\chi^{j2} \left\{ (-2\lambda_{\phi\Omega} v_\Omega + \sqrt{2}\mu_{\phi\Omega}) O_\chi^{k1} - 2\lambda_{\phi\Omega} v_\phi O_\chi^{k2} \right\} \right. \\
& \quad \left. \left. + O_\chi^{j1} \left\{ (-2\lambda_{\phi\Omega} v_\Omega + \sqrt{2}\mu_{\phi\Omega}) O_\chi^{k2} - 6\lambda_\phi v_\phi O_\chi^{k1} \right\} \right] \right\} \quad (\text{A.3})
\end{aligned}$$



$$\begin{aligned}
&= i \left( A_L^{\bar{d}_i d_j h_k} P_L + A_R^{\bar{d}_i d_j h_k} P_R \right) \\
&= -i \frac{1}{\sqrt{2}} O_\chi^{k1} U_{(L)jb}^{d*} U_{(R)ia}^{d*} Y_{(d)}^{ab} P_L \\
&\quad - i \frac{1}{\sqrt{2}} O_\chi^{k1} U_{(R)ja}^d U_{L ib}^d Y_{(d)}^{ab*} P_R \tag{A.4}
\end{aligned}$$

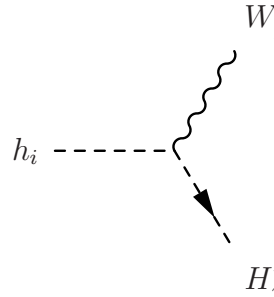


$$\begin{aligned}
&= i \left( A_L^{\bar{u}_i u_j h_k} P_L + A_R^{\bar{u}_i u_j h_k} P_R \right) \\
&= i \frac{1}{\sqrt{2}} O_\chi^{k1} U_{(L)jb}^{u*} U_{(R)ia}^{u*} Y_{(u)}^{ab} P_L \\
&\quad + i \frac{1}{\sqrt{2}} O_\chi^{k1} U_{(R)ja}^u U_{(L)ib}^u Y_{(u)}^{ab*} P_R \tag{A.5}
\end{aligned}$$

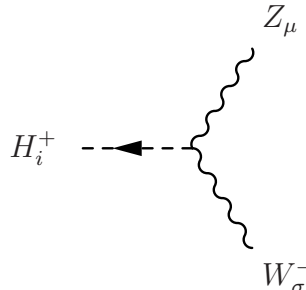


$$\begin{aligned}
&= i \left( A_L^{\bar{e}_i e_j h_k} P_L + A_R^{\bar{e}_i e_j h_k} P_R \right) \\
&= -i \frac{1}{\sqrt{2}} O_\chi^{k1} V_{(L)jb}^{e*} V_{(R)ia}^{e*} Y_{(e)}^{ab} P_L \\
&\quad - i \frac{1}{\sqrt{2}} O_\chi^{k1} V_{(R)ja}^e V_{(L)ib}^e Y_{(e)}^{ab*} P_R
\end{aligned} \tag{A.6}$$

## A.2 Diagrams Involving Charged Higgses



$$\begin{aligned}
&= i O_{h_i H_j^+ W^-} \left( -p^{H_j^+} + p^{h_i} \right)_\mu \\
&= \frac{i}{2} g_2 \left( -2 O_\chi^{i2} O_c^{j2} + O_\chi^{i1} O_c^{j1} \right) \left( -p^{H_j^+} + p^{h_i} \right)_\mu
\end{aligned} \tag{A.7}$$



$$\begin{aligned}
&= i O_{H_j^+ W^- Z} g_{\sigma\mu} \\
&= -\frac{i}{2} g_{\sigma\mu} \left( 2g_2^2 v_\Omega O_c^{i2} \cos \Theta_W + g_1 g_2 v_\phi O_c^{i1} \sin \Theta_W \right)
\end{aligned} \tag{A.8}$$

$$\begin{aligned}
&= i \left( A_L^{\bar{u}_i d_j H_k^+} P_L + A_R^{\bar{u}_i d_j H_k^+} P_R \right) \\
&= -i \left( U_{(L)jb}^{d,*} U_{(R)ia}^{u,*} Y_u^{ab} O_\chi^{k1} P_L + U_{(R)ja}^d U_{(L)ib}^u Y_d^{ab*} O_\chi^{k1} P_R \right) \quad (\text{A.9})
\end{aligned}$$

$$\begin{aligned}
&= i \left( A_L^{\bar{\nu}_i e_j H_k^+} P_L + A_R^{\bar{\nu}_i e_j H_k^+} P_R \right) \\
&= -i V_{(R)ja}^e V_{ib}^\nu Y_e^{ab*} O_c^{k1} P_R \quad (\text{A.10})
\end{aligned}$$



## References

- [1] P. W. Higgs, *Rev. Mod. Phys.* **86**, 851 (2014).
- [2] T. Kajita, *Rev. Mod. Phys.* **88**, 030501 (2016).
- [3] A. B. McDonald, *Rev. Mod. Phys.* **88**, 030502 (2016).
- [4] D. Forero, M. Tortola, and J. W. F. Valle, *Phys.Rev.* **D90**, 093006 (2014), 1405.7540.
- [5] J. W. F. Valle and J. C. Romao, *Neutrinos in high energy and astroparticle physics* (John Wiley & Sons, 2015).
- [6] G. Bertone, *Particle dark matter; observations, models and searches* (Cambridge University Press, 2010).
- [7] M. Hirsch, S. Morisi, E. Peinado, and J. W. F. Valle, *Phys.Rev.* **D82**, 116003 (2010), 1007.0871.
- [8] M. Boucenna, S. Morisi, E. Peinado, Y. Shimizu, and J. W. F. Valle, (2012), 1204.4733.
- [9] L. Lavoura, S. Morisi, and J. W. F. Valle, *JHEP* **1302**, 118 (2013), 1205.3442.
- [10] S. C. Chuliá, R. Srivastava, and J. W. F. Valle, *Phys. Lett.* **B761**, 431 (2016), 1606.06904.
- [11] V. Berezinsky and J. W. F. Valle, *Phys. Lett.* **B318**, 360 (1993), hep-ph/9309214.
- [12] M. Lattanzi and J. W. F. Valle, *Phys. Rev. Lett.* **99**, 121301 (2007), arXiv:0705.2406 [astro-ph].
- [13] F. Bazzocchi *et al.*, *JCAP* **0808**, 013 (2008), 0805.2372.
- [14] M. Lattanzi *et al.*, *Phys.Rev.* **D88**, 063528 (2013), 1303.4685.
- [15] E. Ma, *Phys.Rev.* **D73**, 077301 (2006), hep-ph/0601225.
- [16] M. Hirsch *et al.*, *JHEP* **1310**, 149 (2013), 1307.8134.
- [17] A. Merle, M. Platscher, N. Rojas, J. W. F. Valle, and A. Vicente, *JHEP* **07**, 013 (2016), 1603.05685.
- [18] K. Kannike, *Eur. Phys. J.* **C72**, 2093 (2012), 1205.3781.
- [19] G. Aad, *et. al* [ATLAS Collaboration], *Phys. Rev. Lett.* **113**, 17 (2014), hep-ex/1407.6583.
- [20] V. Khachatryan *et. al* [CMS Collaboration], hep-ex/1701.02032.
- [21] G. Aad *et al.* [ATLAS Collaboration], *New J. Phys.* **15**, 043009 (2013), hep-ex/1302.4403.
- [22] J. A. Casas and A. Ibarra, *Nucl. Phys.* **B618**, 171 (2001), hep-ph/0103065.
- [23] J. Schechter and J. Valle, *Phys.Rev.* **D22**, 2227 (1980).
- [24] P. Rocha-Morán and A. Vicente, *JHEP* **1607**, 078 (2016), 1605.01915.
- [25] G. Aad *et al.*, [ATLAS & CMS Collaborations], *Phys. Rev. Lett.* **114**, 191803 (2015), 1503.07589.

- [26] WMAP, C. L. Bennett *et al.*, *Astrophys. J. Suppl.* **208**, 20 (2013), 1212.5225.
- [27] Planck, P. A. R. Ade *et al.*, *Astron. Astrophys.* **594**, A13 (2016), 1502.01589.
- [28] A. Djouadi, A. Falkowski, Y. Mambrini, and J. Quevillon, *Eur. Phys. J.* **C73**, 2455 (2013), 1205.3169.
- [29] M. Hirsch *et al.*, (2012), 1201.5525.
- [30] M. A. Díaz, B. Koch, and S. Urrutia-Quiroga, *Adv. High Energy Phys.* **2016**, 8278375 (2016), 1511.04429.
- [31] C. Bonilla, E. Ma, E. Peinado, and J. W. F. Valle, *Phys. Lett.* **B762**, 214 (2016), 1607.03931.
- [32] J. Alwall *et al.*, *JHEP* **07**, 079 (2014), 1405.0301.
- [33] H. Baer *et al.*, (2013), 1306.6352.
- [34] CLIC Detector and Physics Study, H. Abramowicz *et al.*, *Physics at the CLIC e+e- Linear Collider – Input to the Snowmass process 2013*, in *Proceedings, Community Summer Study 2013: Snowmass on the Mississippi (CSS2013): Minneapolis, MN, USA, July 29-August 6, 2013*, 2013, 1307.5288.
- [35] S. Blunier, G. Cottin, M. A. Díaz, and B. Koch, (2016), 1611.07896.
- [36] W. Porod, *Comput. Phys. Commun.* **153**, 275 (2003), hep-ph/0301101.